

# Evolution of Alfvén wave-driven solar winds to red giants

Takeru K. Suzuki

School of Arts and Sciences, University of Tokyo, Komaba, Meguro, Tokyo, Japan 153-8902  
email: [stakeru@ea.c.u-tokyo.ac.jp](mailto:stakeru@ea.c.u-tokyo.ac.jp)

**Abstract.** In this talk we introduce our recent results of global 1D MHD simulations for the acceleration of solar and stellar winds. We impose transverse photospheric motions corresponding to the granulations, which generate outgoing Alfvén waves. The Alfvén waves effectively dissipate by 3-wave coupling and direct mode conversion to compressive waves in density-stratified atmosphere. We show that the coronal heating and the solar wind acceleration in the open magnetic field regions are natural consequence of the footpoint fluctuations of the magnetic fields at the surface (photosphere). We also discuss winds from red giant stars driven by Alfvén waves, focusing on different aspects from the solar wind. We show that red giants wind are highly structured with intermittent magnetized hot bubbles embedded in cool chromospheric material.

**Keywords.** waves, MHD, Sun: photosphere, Sun: chromosphere, Sun: Corona, solar wind, stars: chromospheres, stars: coroneae, stars: magnetic fields, stars: mass loss, stars: late-type

---

## 1. Introduction

The Alfvén wave, generated by the granulations or other surface activities, is a promising candidate operating in the heating and acceleration of solar winds from coronal holes. It can travel a long distance so that the dissipation plays a role in the heating of the solar wind plasma as well as the lower coronal plasma, in contrast to other processes, such as magnetic reconnection events and compressive waves, the heating of which probably concentrates at lower altitude.

While high-frequency ioncyclotron waves are recently highlighted for the preferential heating of minor heavy ions (Axford & McKenzie 1997) the protons, which compose the main part of the plasma, are supposed to be mainly heated by low-frequency ( $\lesssim 0.1\text{Hz}$ ) components in the MHD regime. because (1) the low-frequency wave is expected to have more power, and (2) the resonance frequency of the proton is higher than those of heavier ions so that the energy of the ioncyclotron wave is in advance absorbed by heavy ions (Cranmer 2000). In this paper, we focus on roles of such low frequency Alfvén waves.

When considering low-frequency Alfvén waves in solar and stellar atmospheres, the stratification of the density due to the gravity is quite important because the variation scale of the density, and accordingly Alfvén speed, is comparable to or shorter than the wavelengths; the WKB approximation is no longer applicable. Also, the amplitude is amplified because of the decrease of the density so that waves easily become nonlinear. Recently, we have extensively studied the heating and acceleration of solar and stellar winds by self-consistent MHD simulations from the photosphere to sufficiently outer region (Suzuki & Inutsuka 2005; 2006; hereafter SI06; Suzuki 2007). We review these works in this contribution talk.

## 2. Simulation

We consider 1D open flux tubes which are super-radially open, measured by heliocentric distance,  $r$ . The simulation regions are from the photosphere (density,  $\rho = 10^{-7} \text{g cm}^{-3}$ , for the Sun) to several stellar radii. Radial field strength,  $B_r$ , is given by conservation of magnetic flux as  $B_r r^2 f(r) = \text{const.}$ , where  $f(r)$  is a super-radial expansion factor (see SI06 for detail).

We input the transverse fluctuations of the field line by the granulations at the photosphere, which excite Alfvén waves. In this paper we only show results of linearly polarized perturbations with power spectrum proportional to  $1/\nu$ , where  $\nu$  is frequency (for circularly polarized fluctuations with different spectra, see SI06). Amplitude,  $\langle dv_{\perp,0} \rangle$ , at the photosphere is chosen to be compatible with the observed photospheric velocity amplitude  $\sim 1 \text{km s}^{-1}$  (Holweg 1978). At the outer boundaries, non-reflecting condition is imposed for all the MHD waves, which enables us to carry out simulations for a long time until quasi-steady state solutions are obtained without unphysical wave reflection.

We dynamically treat the propagation and dissipation of the waves and the heating and acceleration of the plasma by solving ideal MHD equations. In the energy equation we take into account radiative cooling and Spitzer thermal conduction (SI06). We adopt the second-order MHD-Godunov-MOCCT scheme (Sano & Inutsuka 2008 in preparation) to update the physical quantities. We initially set static atmosphere with a temperature  $T = 10^4 \text{K}$  to see whether the atmosphere is heated up to coronal temperature and accelerated to accomplish the transonic flow. At  $t = 0$  we start the inject of the transverse fluctuations from the photosphere and continue the simulations until the quasi-steady states are achieved.

## 3. Results

### 3.1. Fast Solar Wind

Figure 1 plots the initial condition (dashed lines) and the results after the quasi-steady state condition is achieved at  $t = 2573$  minutes (solid lines), compared with recent observations of fast solar winds. We set the transverse fluctuation,  $\langle dv_{\perp,0} \rangle = 0.7 \text{km s}^{-1}$ , and field strength,  $B_{r,0} = 161 \text{G}$  at the photosphere, and the total superradial expansion factor,  $f_{\text{tot}} = 75$ . Figure 1 shows that the initially cool and static atmosphere is effectively heated and accelerated by the dissipation of the Alfvén waves. The sharp transition region which divides the cool chromosphere with  $T \sim 10^4 \text{K}$  and the hot corona with  $T \sim 10^6 \text{K}$  is formed owing to a thermally unstable region around  $T \sim 10^5 \text{K}$  in the radiative cooling function (Landini & Monsignori-Fossi 1990). The hot corona streams out as the transonic solar wind. The simulation naturally explains the observed trend quite well.

The heating and acceleration of the solar wind plasma in inner heliosphere is done by the dissipation of Alfvén waves. Here we inspect waves in more detail. Figure 2 presents contours of amplitude of  $v_r$ ,  $\rho$ ,  $v_{\perp}$ , and  $B_{\perp}/B_r$  in  $R_{\odot} \leq r \leq 15R_{\odot}$  from  $t = 2570$  min. to 2600 min. Red (blue) shaded regions denote positive (negative) amplitude. Above the panels, we indicate the directions of the local 5 characteristics, two Alfvén, two slow, and one entropy waves at the respective positions. Note that the fast MHD and Alfvén modes degenerate in our case (wave vector and underlying magnetic field are in the same direction), so we simply call the innermost and outermost waves Alfvén modes. In our simple 1D geometry,  $v_r$  and  $\rho$  trace the slow modes which have longitudinal wave components, while  $v_{\perp}$  and  $B_{\perp}$  trace the Alfvén modes which are transverse

One can clearly see the Alfvén waves in  $v_{\perp}$  and  $B_{\perp}/B_r$  diagrams, which have the same slopes with the Alfvén characteristics shown above. One can also find the incoming modes

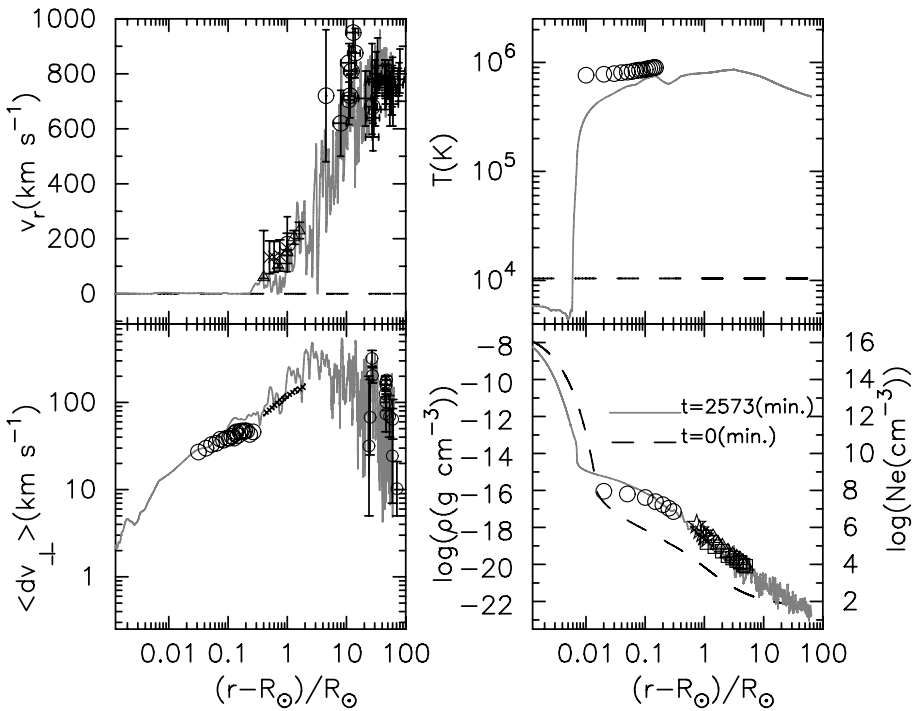


**Figure 1.** Results of fast solar wind mode with observations in polar regions. Outflow speed,  $v_r$  ( $\text{km s}^{-1}$ ) (top-left), temperature,  $T$  (K) (top-right), density in logarithmic scale,  $\log(\rho(\text{g cm}^{-3}))$  (bottom-right), and rms transverse amplitude,  $\langle dv_{\perp} \rangle$  ( $\text{km s}^{-1}$ ) (bottom-left) are plotted. Observational data in the third panel are electron density,  $\log(N_e(\text{cm}^{-3}))$  which is to be referred to the right axis. Dashed lines indicate the initial conditions and solid lines are the results at  $t = 2573$  minutes. In the bottom panel, the initial value ( $\langle dv_{\perp} \rangle = 0$ ) dose not appear. The observational data in the inner region ( $< 6R_{\odot}$ ) are from SOHO (Teriaca et al.2003; Zangrilli et al.2002; Fludra et al.1999; Wilhelm et al.1998; Lamy et al.1997; Banergee et al.1998; Esser et al.1999) and those in the outer region are from interplanetary scintillation measurements (Grall et al.1996; Habbal et al.1994; Kojima et al.2004; Canals et al.2002).

propagating from lower-right to upper-left as well as the outgoing modes generated from the surface. These incoming waves are generated by the reflection at the ‘density mirrors’ of the slow modes. At intersection points of the outgoing and incoming characteristics the non-linear wave-wave interactions take place, which play a role in the wave dissipation.

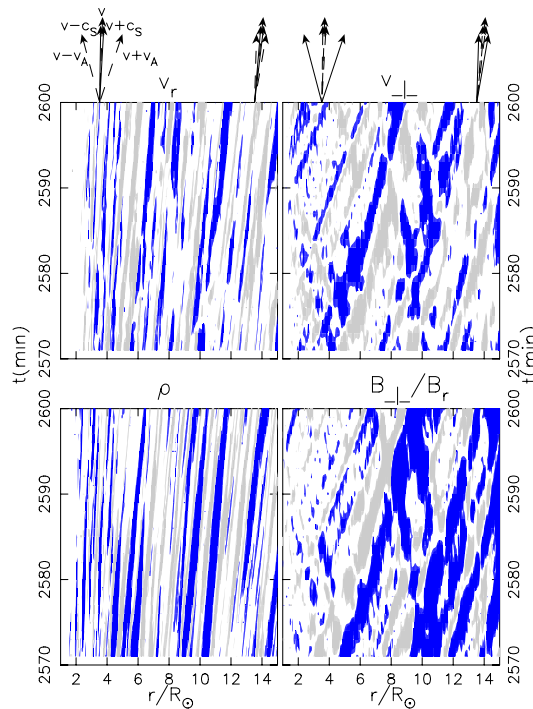
The slow modes are seen in  $v_r$  and  $\rho$  diagrams. Although it might be difficult to distinguish, the most of the patterns are due to the outgoing slow modes† which are generated from the perturbations of the Alfvén wave pressure,  $B_{\perp}^2/8\pi$  (Kudoh & Shibata 1998& Tsurutani et al. 2002). These slow waves steepen eventually and lead to the shock dissipation.

Figure 3 presents the dissipation of the waves more quantitatively. It plots the following quantities,

$$S_c = \rho \delta v^2 \frac{(v_r + v_{ph})^2}{v_{ph}} \frac{r^2 f(r)}{r_c^2 f(r_c)}, \tag{3.1}$$

of outgoing Alfvén , incoming Alfvén , and outgoing slow MHD (sound) waves, where

† The phase correlation of the longitudinal slow waves is opposite to that of the transverse Alfvén waves. The outgoing slow modes have the positive correlation between amplitudes of  $v_r$  and  $\rho$ , ( $\delta v_r \delta \rho > 0$ ), while the incoming modes have the negative correlation ( $\delta v_r \delta \rho < 0$ ).



**Figure 2.**  $r - t$  diagrams for  $v_r$  (upper-left),  $\rho$  (lower-left),  $v_{\perp}$  (upper-right), and  $B_{\perp}/B_r$  (lower-right.) The horizontal axes cover from  $R_{\odot}$  to  $15R_{\odot}$ , and the vertical axes cover from  $t = 2570$  minutes to 2600 minutes. Dark(blue) and light shaded regions indicate positive and negative amplitudes which exceed certain thresholds. The thresholds are  $dv_r = \pm 96 \text{ km/s}$  for  $v_r$ ,  $d\rho/\rho = \pm 0.25$  for  $\rho$ ,  $v_{\perp} = \pm 180 \text{ km/s}$  for  $v_{\perp}$ , and  $B_{\perp}/B_r = \pm 0.16$  for  $B_{\perp}/B_r$ , where  $d\rho$  and  $dv_r$  are differences from the averaged  $\rho$  and  $v_r$ . Arrows on the top panels indicate characteristics of Alfvén, slow MHD and entropy waves at the respective locations.

$\delta v$  and  $v_{\text{ph}}$  are amplitude and phase speed of each wave mode.  $S_c$  is an adiabatic constant derived from wave action (Jacques 1977) in unit of energy flux. For the incoming Alfvén wave, we plot the opposite sign of  $S_c$  so that it becomes positive in the sub-Alfvénic region. The outgoing and incoming Alfvén waves are decomposed by correlation between  $v_{\perp}$  and  $B_{\perp}$ . Extraction of the slow wave is also from fluctuating components of  $v_r$  and  $\rho$ .

Figure 3 clearly illustrates that the outgoing Alfvén waves dissipate quite effectively;  $S_c$  becomes only  $\sim 10^{-3}$  of the initial value at the outer boundary. A sizable amount is reflected back downward below the coronal base ( $r - R_{\odot} < 0.01R_{\odot}$ ), which is known from the incoming Alfvén wave following the outgoing component with slightly smaller level. This is because the wave shape is considerably deformed owing to the steep density gradient; a typical variation scale ( $< 10^5 \text{ km}$ ) of the Alfvén speed becomes comparable to or even shorter than the wavelength ( $= 10^4 - 10^6 \text{ km}$ ). Although the energy flux,  $\simeq 5 \times 10^5 \text{ erg cm}^{-2} \text{ s}^{-1}$ , of the outgoing Alfvén waves ( $S_c$  in the static region is equivalent with the energy flux) which penetrates into the corona is only  $\simeq 15\%$  of the input value, it satisfies the requirement for the energy budget in the coronal holes (Withbroe & Noyes 1977).

The processes discussed here are the combination of the direct mode conversion to the compressive waves and the parametric decay instability due to three-wave (outgoing Alfvén, incoming Alfvén, and outgoing slow waves) interactions (Goldstein 1978;

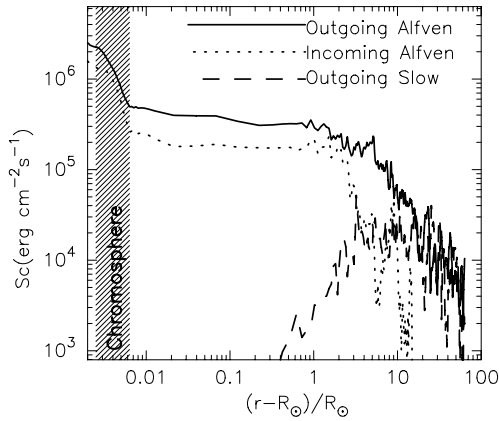


**Figure 3.**  $S_c$  of outgoing Alfvén mode (solid), incoming Alfvén mode (dotted), and outgoing MHD slow mode (dashed) at  $t = 2573$  mins. Hatched region indicates the chromosphere and low transition region with  $T < 4 \times 10^4$  K.

Terasawa et al. 1986) of the Alfvén waves. These processes, which are not generally efficient in homogeneous background, become effective by amplification of velocity amplitude in the density decreasing atmosphere. The Alfvén speed also varies a lot even within one wavelength of Alfvén waves with periods of minutes. This leads to both variation of the wave pressure in one wavelength and partial reflection through the deformation of the wave shape (Moore et al.1991). The density stratification plays a key role in the propagation and dissipation of the Alfvén waves.

### 3.2. Evolution to Red Giant Winds

So far we have focused on the acceleration of solar wind. The same process is expected to operate in other types of stars that have surface convective layer, such as red giant stars, proto-stars, and intermediate and low mass main sequence stars. As a demonstration, we have applied our solar wind simulations to red giant winds (Suzuki 2007).

We consider stellar winds from  $1M_\odot$  stars in various evolutionary stages from main sequence to red giant branch. The properties of surface fluctuations (e.g. amplitude and spectrum) can be estimated from conditions of surface convection which depend on surface gravity and temperature (e.g. Renzini et al.1977; Stein et al. 2004). Then, we carry out the simulations of the red giant winds in a similar manner to the solar wind simulations.

Figure 4 presents the evolution of stellar winds of a  $1M_\odot$  star from main sequence to red giant stages. The middle panel shows that the average temperature drops suddenly from  $T \simeq 7 \times 10^5$  K in the sub-giant star (blue) to  $T \leq 10^5$  K in the red giant stars, which is consistent with the observed “dividing line” (Linsky & Haisch 1979). The main reason of the disappearance of the steady hot coronae is that the sound speed ( $\approx 150 \text{ km s}^{-1}$ ) of  $\approx 10^6$  K plasma exceeds the escape speed,  $v_{\text{esc}}(r) = \sqrt{2GM_\star/r}$ , at  $r \gtrsim$  a few  $R_\star$  in the red giant stars; the hot corona cannot be confined by the gravity any more in the atmospheres of the red giant stars. Therefore, the material flows out before heated up to coronal temperature.

In addition, the thermal instability of the radiative cooling function (Landini & Monsignori-Fossi 1990) plays a role in the sudden decrease of temperature. Because of the thermal instability, magnetized hot ( $\gtrsim 10^6$  K) bubbles intermittently exist in red giant winds, while most of the wind material consist of cool ( $\lesssim 10^4$  K) chromospheric gas (Suzuki 2007).

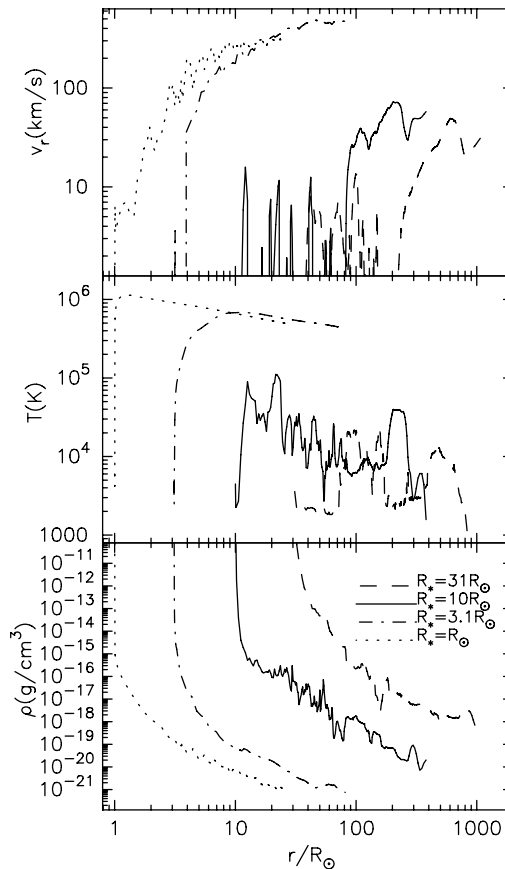


**Figure 4.** Time-averaged stellar wind structure of the  $1M_{\odot}$  stars. From the top to the bottom, radial outflow velocity,  $v_r$  ( $\text{km s}^{-1}$ ), temperature,  $T$  (K), and density,  $\rho$  ( $\text{g cm}^{-3}$ ), are plotted. The black, blue, green, and red lines are the results of stellar radii,  $R = R_{\odot}$  (the present Sun),  $3.1R_{\odot}$  (sub-giant),  $10R_{\odot}$  (red giant), and  $31R_{\odot}$  (red giant), respectively.

#### 4. conclusions

We have performed 1D MHD numerical simulations of solar and stellar winds from the photosphere. The low-frequency Alfvén waves are generated by the footpoint fluctuations of the magnetic field lines. We have treated the wave propagation and dissipation, and the heating and acceleration of the plasma in a self-consistent manner. Our simulation is the first simulation which treats the wind from the real surface (photosphere) to the (inner) heliosphere with the relevant physical processes.

We have shown that the dissipation of the low-frequency Alfvén waves through the generation of the compressive waves (decay instability) and shocks (nonlinear steepening) is one of the solutions for the heating and acceleration of the plasma in the coronal holes. However, we should cautiously examine the validity of the 1-D MHD approximation we have adopted. There are other dissipation mechanisms due to the multidimensionality, such as turbulent cascade into the transverse direction (Goldreich & Sridhar 1995; Oughton et al. 2001) and phase mixing (Heyvaerts & Priest 1983). If Alfvén waves cascade to higher frequency, kinetic effects (e.g. Nariyuki & Hada 2006) becomes important.

We have also extended the solar wind simulations to red giant winds. With stellar evolution, the steady hot corona with temperature,  $T \approx 10^6$  K, suddenly disappears because

the surface gravity becomes small; hot plasma cannot be confined by the gravity. Thermal instability also generate intermittent magnetized hot bubbles in cool chromospheric winds.

### Acknowledgements

The author thanks the organizers of IAU247 for the nice conference. This work is supported in part by a Grant-in-Aid for Scientific Research (19015004) from the Ministry of Education, Culture, Sports, Science, and Technology of Japan.

### References

- Axford, W. I. & McKenzie, J. F. 1997 The Solar Wind in "Cosmic Winds and the Heliosphere", Eds. Jokipii, J. R., Sonnet, C. P., and Giampapa, M. S., University of Arizona Press, 31
- Banerjee, D., Teriaca, L., Doyle, J. G., & Wilhelm, K. 1998 *A&A*, 339, 208
- Canals, A., Breen, A. R., Ofman, L., Moran, P. J., & Fallows, R. A., 2002 *Ann. Geophys.*, 20, 1265
- Cranmer, S. R., 2000, *ApJ*, 532, 1197
- Esser, R., Fineschi, S., Dobrzycka, D., Habbal, S. R., Edgar, R. J., Raymond, J. C., & Kohl, J. L., 1999 *ApJ*, 510, L63
- Fludra, A., Del Zanna, G. & Bromage, B. J. L., 1999 *Spa. Sci. Rev.*, 87, 185
- Goldreich, P. & Sridhar, S., 1995 *ApJ*, 438, 763
- Goldstein, M. L., 1978, *ApJ*, 219, 700
- Grall, R. R., Coles, W. A., Klinglesmith, M. T., Breen, A. R., Williams, P. J. S., Markkanen, J., & Esser, R., 1996 *Nature*, 379, 429
- Habbal, S. R., Esser, R., Guhathakura, M., & Fisher, R. R., 1994 *Gephys. Res. Lett.*, 22, 1465
- Heyvaerts, J. & Priest, E. R., 1983 *A&A*, 117, 220
- Holweger, H., Gehlsen, M., & Ruland, F., 1978 *A&A*, 70, 537
- Jacques, S. A. 1977, *ApJ*, 215, 942
- Kojima, M., Breen, A. R., Fujiki, K., Hayashi, K., Ohmi, T., & Tokumaru, M., 2004 *J. Geophys. Res.*, 109, A04103
- Kudoh, T. & Shibata, K., 1999 *ApJ*, 514, 493
- Lamy, P., Quemerais, E., Liebaria, A., Bout, M., Howard, R., Schwenn, R., & Simnett, G., 1997 Fifth SOHO Workshop, The Corona and Solar Wind near Minimum Activity, ed A. Wilson (ESA-SP 404; Noordwijk:ESA), 491
- Landini, M. & Monsignori-Fossi, B. C., 1990 *A&AS*, 82, 229
- Linsky, J. L. & Haisch, B. M., 1979 *ApJ*, 229, L27
- Moore, R. L., Suess, S. T., Musielak, Z. E., & An, A.-H., 1991 *ApJ*, 378, 347
- Nariyuki, Y. & Hada, T., 2006 *Phys. Plasma*, 13, 124501
- Oughton, S., Matthaeus, W. H., Dmitruk, P., Milano, L. J., Zank, G. P., & Mullan, D. J., 2001 *ApJ* 551, 565
- Renzini, A., Cacciari, C., Ulmschneider, P., & Schmitz, F., 1977 *A&A*, 61, 39
- Stein, R. F., Georgobiani, D., Trampedach, R., Ludwig, H.-G., & Nortlund, Å., 2004, *Sol. Phys.*, 220, 229
- Suzuki, T. K., 2007 *ApJ*, 659, 1592
- Suzuki, T. K. & Inutsuka, S., 2005 *ApJ*, 632, L49
- Suzuki, T. K. & Inutsuka, S., 2006 *J. Geophys. Res.*, 111, A6, A06101
- Terasawa, T., Hoshino, M., Sakai, J. I., & Hada, T., 1986, *J. Geophys. Res.*, 91, 4171
- Teriaca, L., Poletto, G., Romoli, M., & Biesecker, D. A., 2003 *ApJ*, 588, 566
- Tsurutani, B. T. et al., 2002 *Geophys. Res. Lett.*, 29, 23-1
- Wilhelm, K., Marsch, E., Dwivedi, B. N., Hassler, D. M., Lemaire, P., Gabriel, A. H., & Huber, M. C. E., 1998 *ApJ*, 500, 1023
- Withbroe, G. L. & Noyes, R. W., 1977, *ARAA*, 15, 363
- Zangrilli, L., Poletto, G., Nicolosi, P., Noci, G., & Romoli, M., 2002 *ApJ*, 574, 477